ANNUAL REVIEWS

Annual Review of Marine Science

Sediment Trapping in Estuaries

Hans Burchard,[1] Henk M. Schuttelaars,[2] and David K. Ralston[3]

[1]Department of Physical Oceanography and Instrumentation, Leibniz Institute for Baltic Sea Research Warnemünde, D-18119 Rostock, Germany;
email: hans.burchard@io-warnemuende.de

[2]Delft Institute of Applied Mathematics, Delft University of Technology, NL-2628 CD Delft, The Netherlands

[3]Department of Applied Ocean Physics and Engineering, Woods Hole Oceanographic Institution, Woods Hole, Massachusetts 02543, USA

Annu. Rev. Mar. Sci. 2018. 10:371–95

First published as a Review in Advance on October 4, 2017

The *Annual Review of Marine Science* is online at marine.annualreviews.org

https://doi.org/10.1146/annurev-marine-010816-060535

Keywords

estuarine turbidity maxima, suspended particulate matter, tidal estuaries, bottom sediment pool, salt intrusion limit, topographic trapping, hyperturbid estuaries

Abstract

Estuarine turbidity maxima (ETMs) are generated by a large suite of hydrodynamic and sediment dynamic processes, leading to longitudinal convergence of cross-sectionally integrated and tidally averaged transport of cohesive and noncohesive suspended particulate matter (SPM). The relative importance of these processes for SPM trapping varies substantially among estuaries depending on topography, fluvial and tidal forcing, and SPM composition. The high-frequency dynamics of ETMs are constrained by interactions with the low-frequency dynamics of the bottom pool of easily erodible sediments. Here, we use a transport decomposition to present processes that lead to convergent SPM transport, and review trapping mechanisms that lead to ETMs at the landward limit of the salt intrusion, in the freshwater zone, at topographic transitions, and by lateral processes within the cross section. We use model simulations of example estuaries to demonstrate the complex concurrence of ETM formation mechanisms. We also discuss how changes in SPM trapping mechanisms, often caused by direct human interference, can lead to the generation of hyperturbid estuaries.

1. INTRODUCTION

Estuarine turbidity maximum (ETM): a region along an estuary with a localized maximum in tidally and cross-sectionally averaged SPM concentration

Suspended particulate matter (SPM): inorganic and organic fractions of particulate matter suspended in the water column, the largest fraction of which is generally sediment of lithogenic origin

Estuaries have long been recognized as efficient traps for fluvial and marine sediments (Meade 1969), leading to estuarine turbidity maxima (ETMs) with high concentrations of suspended particulate matter (SPM). Such high concentrations often correspond to locations of enhanced deposition that can limit navigation to harbors situated along the estuaries. Direct human interventions, such as deepening and narrowing (Winterwerp & Wang 2013), can lead to enhanced local concentrations of SPM, which can impair optimal functioning of estuarine ecosystems and have multiple environmental and societal implications (Simenstad et al. 1994). Because a fraction of the SPM consists of organic matter that can be bacterially degraded, oxygen consumption may lead to suboxic conditions (Etcheber et al. 2007). Owing to the high turbidity in ETMs, primary production might be inhibited (Yoshiyama & Sharp 2006), which potentially further decreases oxygen concentration levels.

After Glangeaud (1938) first described the ETM in the Gironde estuary, it became clear that ETMs are ubiquitous features in estuaries. **Figure 1** shows some example observations of SPM concentration and salinity for the Elbe, Ems, and Hudson estuaries. In each case, distinct ETM regions have concentrations 5–100 times greater than those at the seaward limit or the river upstream. In the Elbe, the ETM is located near the landward tip of the salt wedge (Kappenberg & Grabemann 2001), whereas in the Ems, the ETM is smeared out far into the freshwater zone (Talke et al. 2009). In the Hudson, multiple ETMs are located within the estuarine salinity gradient and at the landward limit of salt (Ralston et al. 2012).

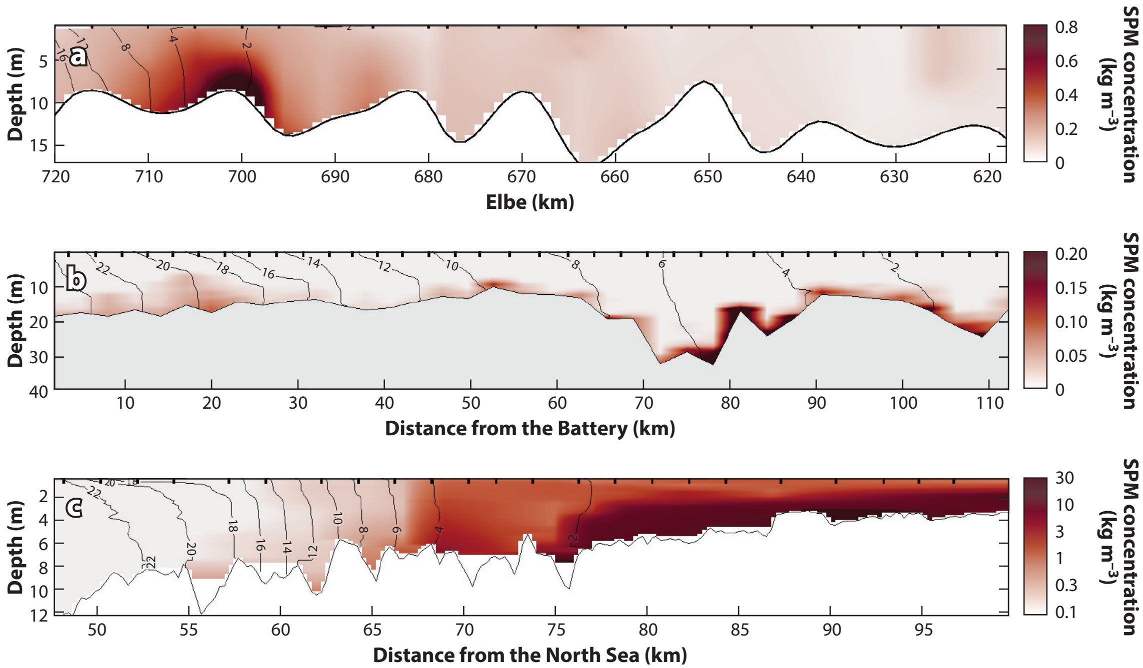

Figure 1

Observational evidence of ETMs, showing the SPM concentration (*color shading*) and salinity (*isolines*). (*a*) Elbe estuary on March 29, 1990, at a high discharge of 707 m^3 s^{-1}. (*b*) Hudson estuary on August 29, 1995, during low-runoff conditions. (*c*) Ems estuary on August 2, 2006, during ebb tide. Abbreviations: ETM, estuarine turbidity maximum; SPM, suspended particulate matter. Data for panel *a* were provided by Jens Kappenberg, Helmholtz-Zentrum Geesthacht, Germany; data for panel *c* are from Talke et al. (2009).

The characteristics of ETMs vary greatly with external forcing, bathymetry, sources of sediment, sediment properties, and hydrodynamic processes. The distribution of bed sediment and SPM in the water column within an estuary depends on the temporal variation and spatial structure of these characteristics. ETM generation mechanisms have been studied by numerous researchers, beginning with Postma & Kalle (1955). Several reviews on ETM dynamics have marked the progress in understanding their complex formation mechanisms (e.g., Dyer 1988; Jay et al. 1997, 2015; Uncles et al. 2002).

The intention of this review is to present and explain the important mechanisms of SPM trapping in estuaries, incorporating recent developments in our understanding of the physical processes from observational and modeling studies. We do this in a systematic way by analyzing the underlying conservation laws of mass, momentum, and SPM. The relevant processes are reviewed and quantitatively synthesized based on simplified models using analytical and numerical solutions, backed up by data from field surveys and realistic numerical models. This discussion includes interactions between bed sediments and SPM in the water column, multiple ETM generation mechanisms, the role of lateral processes, and timescales of variability, as well as the occurrence of hyperturbid estuaries.

2. PHENOMENOLOGY OF ESTUARINE TURBIDITY MAXIMA

ETMs are the result of complex estuarine dynamics leading to convergent transports of SPM, which are highly variable in time and space and differ substantially among estuaries (**Figure 1**). Multiple ETMs are often observed at the same time, as in the Elbe and the Hudson (**Figure 1**) as well as in other estuaries, including those of the Columbia River (Jay & Musiak 1994), the York River (Lin & Kuo 2001), and the Ems (de Jonge et al. 2014). Despite the complexity, some general relations have been found for ETM dynamics. In a comparative study of 44 tidal estuaries, Uncles et al. (2002) showed that the maximum SPM concentration and residence time in ETMs depend on two parameters: mean spring tidal range and tidal length. Comparing 15 estuaries, Jay et al. (2007b) found that the trapping efficiency is negatively correlated to the fluvial forcing characterized by the supply number (settling velocity scaled by runoff velocity).

Despite their high diversity, we start by describing the dominant types of ETMs, including those created by longitudinal convergence, such as at the landward limit of the salt intrusion (Section 2.1), in the freshwater zone (Section 2.2), and at topographic transitions (Section 2.3). Trapping in the lateral direction is discussed in Section 2.4.

2.1. Estuarine Turbidity Maxima at the Salt Intrusion Limit

The first systematic investigation of ETMs occurring at the landward limit of the salt intrusion was carried out by Postma & Kalle (1955) for the Elbe estuary (see also Postma 1967). They hypothesized that "the mixing of river and marine waters in the tidal zone acts as a suspended matter trap, leading to enrichment of suspended matter in the water as well as at the bottom of the mixing zone" (p. 143; our translation). They also explained the trapping mechanism by the fact that "whereas the light river water flows toward the sea preferably in near-surface layers, the heavy, salty seawater flows landward in deep layers above the bottom" (p. 143; our translation). In essence, this means that estuarine circulation is responsible for ETM formation. Festa & Hansen (1978) were the first to systematically investigate ETM formation at the landward limit of the salt intrusion using an idealized numerical model, parameterizing the effects of tides by constant mixing coefficients. They showed that the trapping efficiency is mainly a function of the settling velocity and the strength of the estuarine circulation. Burchard & Baumert (1998) applied

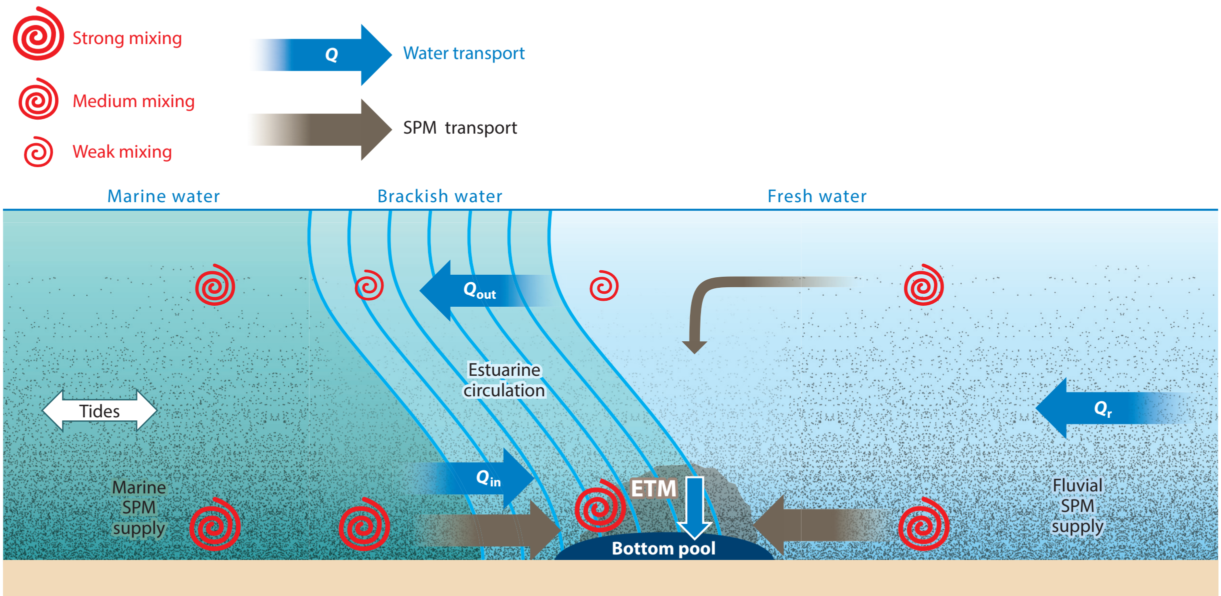

Figure 2

Major processes for sediment transport convergence that lead to ETM formation at the landward limit of the salt intrusion. Abbreviations: ETM, estuarine turbidity maximum; SPM, suspended particulate matter.

a tidally resolved model, including a dynamic turbulence closure scheme, to show that several processes in addition to gravitational circulation contribute to SPM trapping, such as increased estuarine circulation caused by eddy viscosity and vertical shear covariance (Jay & Musiak 1994), suppression of vertical turbulent SPM transport caused by stable stratification (Geyer 1993), and tidal covariance of velocity and SPM concentration (Scully & Friedrichs 2007).

Figure 2 illustrates the classical mechanisms for ETMs developing at the landward limit of the salt intrusion. The estuarine salinity gradient in concert with the river runoff drives an estuarine circulation that can be quantified using the Knudsen relation (Knudsen 1900, MacCready & Geyer 2010) with a near-bottom up-estuary volume transport Q_{in}, which is confined to the region of the salinity gradient; the river runoff Q_{r}; and the near-surface outflow transport Q_{out}, with the long-term balance $Q_{\mathrm{out}} = Q_{\mathrm{in}} + Q_{\mathrm{r}}$. This estuarine circulation drives an up-estuary SPM transport (see Section 3.1) that extends to the landward limit of the salt intrusion, where it ceases abruptly because the internal pressure gradient vanishes. This process alone establishes a convergent SPM transport that leads to increased SPM concentrations and the formation of an ETM. SPM from riverine sources is transported downstream by the mean flow until it reaches the upstream near-bottom transport in the salinity gradient, leading to the convergence of SPM transport at the landward limit of the salt intrusion.

2.2. Estuarine Turbidity Maxima in the Freshwater Zone

Decades after the effect of the salinity gradient on SPM transport was recognized, the possibility that purely tidal processes could result in SPM trapping was first discussed in 1980 for the Gironde and Aulne estuaries (Allen et al. 1980). During periods of low river flow, a well-developed turbidity maximum is often maintained in the freshwater zone in these estuaries because of tidal transport mechanisms, whereas the gravitational circulation dominates the trapping processes during high river flow. The ETM locations can vary by 30–40 km depending on river discharge and tidal forcing conditions, and the ETMs are not necessarily located at the limit of the salinity intrusion.

Focusing on the trapping of SPM in the freshwater zone of the Gironde, Allen et al. (1980) identified the asymmetry between the peak ebb and flood velocities (resulting from the deformation of the tidal wave when propagating into the estuary) as the main upstream transport mechanism, together with transport caused by tidal duration asymmetry (see Section 3.2), balancing the downstream transport caused by river discharge. The importance of barotropic, tide-induced SPM transport and trapping was later discussed for many other estuaries (see, e.g., Uncles & Stephens 1993, Dyer 1997, Brenon & Le Hir 1999, Chernetsky et al. 2010, Yu et al. 2014).

2.3. Topographic Trapping

Observations in numerous estuaries have found that ETMs are not necessarily associated with the limit of salinity or of tidal propagation, but rather are spatially fixed and associated with bathymetric transitions. In northern San Francisco Bay, ETMs are located near straits where baroclinic circulation and stratification are locally intensified and are not tied to a particular salinity (Schoellhamer 2000). In the Columbia River, persistent ETMs are also present at narrow, deep holes and are spatially locked compared with the salinity variability with river discharge and tidal amplitude (Jay & Musiak 1994, Fain et al. 2001, Hudson et al. 2017). In the Delaware, an ETM is located near a rapid expansion, where decreases in river and tidal velocity lead to SPM convergence (Sommerfield & Wong 2011). ETMs that are spatially locked at topographic transitions independent of salinity have also been noted in Chesapeake Bay (North & Houde 2001), the Elbe (Kappenberg & Grabemann 2001), the York (Lin & Kuo 2001), and the Hudson (Geyer et al. 2001).

In the Hudson, the strongest ETM occurs in the middle of the salinity gradient (at 20 km in **Figure 1*b***), where a constriction leads to baroclinic trapping and SPM concentrations greater than 1 g L^{-1} during the spring freshet (Panuzio 1965, Geyer et al. 2001). During lower discharge, salinity extends farther landward and a second ETM develops (at 55 km in **Figure 1*b***) that is also topographically locked to a channel constriction (Ralston et al. 2012). Both ETMs are generated by local intensification of baroclinic circulation and stratification at bottom salinity fronts downstream from constrictions (Ralston et al. 2012, Geyer & Ralston 2015), leading to accumulation of fine sediment (Woodruff et al. 2001, Nitsche et al. 2010). The prevalence of topographically controlled ETMs in other estuaries suggests that these processes of frontogenesis provide a mechanism for SPM convergence that is dynamically similar to the fresh water–salt water interface but can occur at any salinity and enhance trapping throughout the estuary.

2.4. Lateral Trapping Processes

The longitudinal and lateral transport and trapping of SPM are fundamentally linked (Fugate et al. 2007, McSweeney et al. 2016). Here, we review several processes that result in lateral trapping.

Lateral depth variations result in laterally varying bottom stresses and consequently a coarser bed in the deeper parts and an accumulation of fines on the shoals (Geyer et al. 2001, Lin & Kuo 2001, McSweeney et al. 2016). Lateral depth gradients can also correspond with lateral gradients in stratification, affecting bottom stress and resuspension, as is the case, for example, in the York River (Scully & Friedrichs 2007) and Delaware River (McSweeney et al. 2016).

Differential advection of the along-estuary salinity gradient during the flood tide creates lateral salinity gradients that transport near-bed sediment out of the channel toward the shoals (Geyer et al. 1998). During ebbs, the oblique projection of along-estuary fronts at channel expansions creates a lateral baroclinic pressure gradient with the same sense as differential advection and, correspondingly, a convergence in suspended sediment at the transition between channel and shoal, where the front intersects the bed (Ralston et al. 2012). Trapping by lateral circulation alters the lateral distribution of bed sediment and therefore is fundamentally linked to the along-estuary SPM transport.

Coriolis acceleration also creates lateral circulation and sediment trapping primarily through lateral salinity gradients, driving SPM toward the right shoals in the Northern Hemisphere (Huijts et al. 2006, Chen & Sanford 2009, McSweeney et al. 2016). Channel curvature causes centrifugal acceleration that is dynamically similar to Coriolis acceleration and moves sediment toward the shoals and inside of the bend. Lateral circulation mechanisms can interact, as seen in Winyah Bay with differential advection and Coriolis acceleration (Kim & Voulgaris 2008) and in Chesapeake Bay with channel curvature and Coriolis acceleration (Fugate et al. 2007).

Lateral trapping can extend to tidal flats and shallow side embayments, where sediment deposited during high discharge can be remobilized back to the main channel during lower discharge (Fain et al. 2001, Le Hir et al. 2001, Yellen et al. 2017). Generally, lateral trapping by salinity gradients or advective processes such as settling lag (Yang et al. 2014) move fine sediment toward the shoals, resulting in greater SPM resuspension and affecting the lateral distribution of along-estuary transport.

3. MATHEMATICAL DESCRIPTION OF SEDIMENT TRAPPING

To quantitatively evaluate the general ETM formation processes described in the previous section, we briefly present here the mathematical framework for SPM transport and convergence.

3.1. Dynamic Equations

To quantitatively understand SPM trapping in estuaries, it is sufficient to consider SPM as a single class (for short discussions of models with multiple classes, see, e.g., McAnally & Mehta 2002, Jay et al. 2007a). In this approach, the SPM dynamics are described by

$$\frac{\partial c}{\partial t} + \frac{\partial (uc)}{\partial x} + \frac{\partial (vc)}{\partial y} + \frac{\partial [(w - w_s)c]}{\partial z} - \frac{\partial}{\partial z}\left(K_v \frac{\partial c}{\partial z}\right) = P, \qquad 1.$$

where c is the mass fraction of SPM in grams per liter (equivalent to kilograms per cubic meter), i.e., SPM dry mass per water volume; (u, v, w) is the three-dimensional Cartesian velocity vector; w_s is the settling velocity of SPM; and K_v is the eddy diffusivity. Horizontal diffusive terms are not shown here. The term P on the right-hand side denotes nonconservative processes, such as sources resulting from primary production or sinks resulting from mineralization of organic SPM fractions (e.g., Cerco et al. 2013). A Cartesian coordinate system is used, where the space vector (x, y, z) is oriented with x pointing in the up-estuary direction, y pointing across the estuary to the left (looking into the estuary), and z pointing upward. The vertical coordinate z ranges from $z = -H(x, y, t)$ to $z = \eta(x, y, t)$, where $H(x, y, t)$ is the undisturbed water depth and $\eta(x, y, t)$ is the surface elevation.

The budget Equation 1 incorporates the continuum assumption, i.e., that SPM can be considered as a concentration instead of as particles. Sediment settling, which usually varies in space and time, is an essential process in estuarine sediment trapping. However, most basic ETM dynamics can be explained by just assuming a constant settling velocity (e.g., Festa & Hansen 1978, Allen et al. 1980). For high SPM concentrations (see Section 8.1), the cohesiveness of sediments begins to play a substantial role, with the settling velocity depending on the SPM concentration and on the turbulence intensity capturing processes such as hindered settling and flocculation (Winterwerp 1998, 2001).

The boundary condition at the free surface results from the requirement that the normal SPM flux vanishes:

$$-w_s c - K_v \frac{\partial c}{\partial z} = 0 \quad \text{for} \quad z = \eta. \qquad 2.$$

The SPM flux normal to the bottom equals the difference between the erosion flux F_e and deposition flux F_s:

$$-w_s c - K_v \frac{\partial c}{\partial z} = F_e - F_s \quad \text{for} \quad z = -H, \qquad 3.$$

assuming small surface and bottom slopes (Kumar et al. 2017). Most models allow for continuous deposition (Winterwerp & van Kesteren 2004, Sanford 2008), resulting in $F_s = w_s c$, with c evaluated at $z = -H$. Equation 3 then reduces to $-K_v \partial c / \partial z = F_e$.

Bottom pool: a mobile pool of easily erodible SPM that has settled at the bottom, quantified as dry weight per area

Observations suggest that the ETM formation leads to the accumulation of a pool of easily erodible sediment on the seabed (Wellershaus 1981, Geyer 1993). Neglecting consolidation on long timescales, the evolution equation for this bottom pool B is

$$\frac{\partial B}{\partial t} = F_s - F_e \qquad 4.$$

(for details, see Burchard & Baumert 1998, Burchard et al. 2013). If the tidally averaged B is time independent, the system is said to be in morphodynamic equilibrium (Friedrichs et al. 1998, Huijts et al. 2006, Chernetsky et al. 2010). For erosion, the well-accepted Ariathurai-Partheniades formulation is combined with the formulation for limited bed sediment availability ($B = 0$):

$$F_e = \begin{cases} \hat{M} & \text{for } B > 0 \\ \min\{F_s, \hat{M}\} & \text{for } B = 0 \end{cases} \quad \text{with} \quad \hat{M} = M \max\left\{ \frac{(u_{*,b})^2}{(u_c)^2} - 1, 0 \right\} \qquad 5.$$

(see Ariathurai 1974), where $u_{*,b}$ is the bed friction velocity, u_c is the critical bed friction velocity, and M is a constant erosion rate parameter.

3.2. Tidal and Spatial Averaging

SPM trapping in estuaries is a consequence of convergent transports, so the underlying mechanisms can first be examined by studying along-estuary gradients of the cross-sectionally integrated SPM transport. Integrating the SPM transport described by Equation 1 over the cross-sectional area A, tidally averaging, and using the bottom pool described by Equation 4 and integrated over width W (for details, see **Supplemental Appendix 1**) results in

Supplemental Material

$$\frac{\partial}{\partial t}\left(W \langle [B]_y \rangle + \langle A[c]_A \rangle\right) = -\frac{\partial}{\partial x} \langle A[uc]_A \rangle + \left\langle D_r [F_r^{lat}]_z \right\rangle - \left\langle D_l [F_l^{lat}]_z \right\rangle + \langle A[P]_A \rangle, \qquad 6.$$

where $[\cdot]_y$, $[\cdot]_z$, and $[\cdot]_A$ denote lateral, vertical, and cross-sectional averages, respectively, and $\langle\cdot\rangle$ denotes a tidal average. F_r^{lat} and F_l^{lat} are the respective lateral SPM transports on the right and left side, and D_r and D_l are the respective water depths at the lateral banks. Equation 6 shows that the tidally averaged, cross-sectionally integrated amount of easily erodible SPM (in the water column and bottom pool) changes on subtidal timescales owing to the convergence of tidally averaged SPM transport, transport through the lateral boundaries, and production.

Integration of Equation 6 along an estuarine segment of length L including a water volume V results in

$$\frac{\partial}{\partial t}\left(W L \langle [[B]_y]_x \rangle + \langle V [c]_V \rangle\right) = -\langle A[uc]_A \rangle_{up} + \langle A[uc]_A \rangle_{down} + \langle \mathcal{F}_L^{lat} \rangle + \langle \mathcal{P} \rangle, \qquad 7.$$

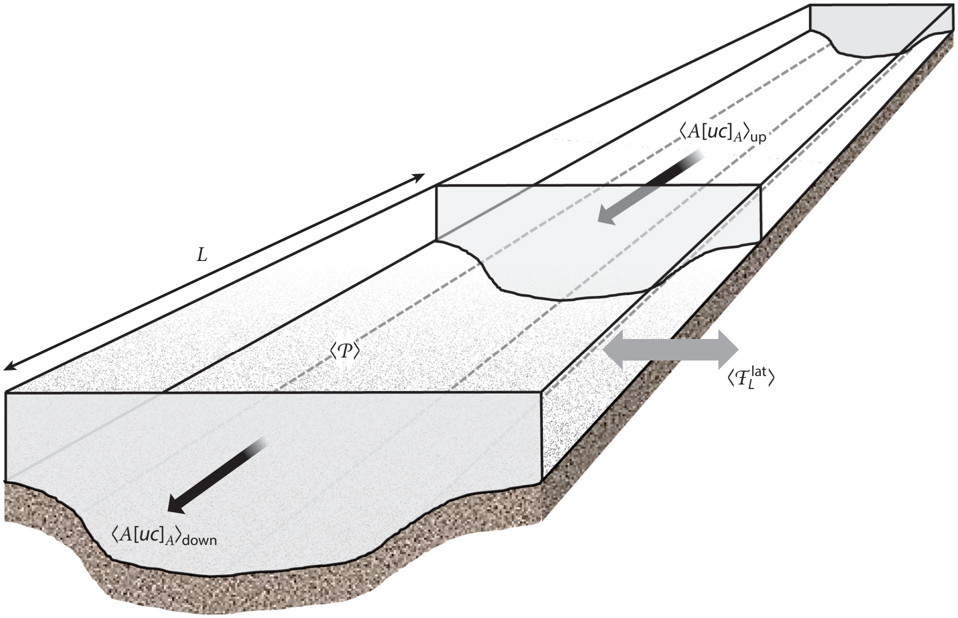

Figure 3

The processes in an estuarine segment of length L as quantified in Equation 7. $\langle A[uc]_A\rangle_{\mathrm{up}}$ and $\langle A[uc]_A\rangle_{\mathrm{down}}$ are the upstream and downstream cross-sectionally averaged SPM transports, respectively; $\langle \mathcal{F}_L^{\mathrm{lat}}\rangle$ denotes the lateral net fluxes of sediment; and $\langle \mathcal{P}\rangle$ denotes the volume-integrated, tidally averaged SPM production. Abbreviation: SPM, suspended particulate matter.

Supplemental Material

where $\langle \mathcal{F}_L^{\mathrm{lat}}\rangle$ includes all lateral SPM transports and $\langle \mathcal{P}\rangle$ is the volume-integrated, tidally averaged SPM production (for details, see **Supplemental Appendix 1**). Equation 7 shows that the change of total SPM contained in an estuarine segment depends largely on the divergence (or convergence) of integrated transports across the upstream and downstream cross sections and lateral boundaries as well as on the local production or decomposition of SPM. **Figure 3** illustrates the relevant SPM transports.

3.3. Sediment Transport Decomposition

As Equation 7 shows, the convergence of cross-sectionally integrated and tidally averaged SPM transport across an estuarine cross section, $\langle A[uc]_A\rangle$, is key to understand SPM accumulation and ETM formation in estuaries. To highlight the relevant underlying processes, several authors (Fischer 1972, Uncles et al. 1985, Dyer 1988, Díez-Minguito et al. 2014, Becherer et al. 2016) have proposed decompositions of this transport, of which one form is the following:

$$\begin{aligned}\langle A[uc]_A\rangle &= \underbrace{W\left[\langle D[uc]_z\rangle\right]_y}_{\mathcal{T}}\\ &= \underbrace{W\left[\langle D\rangle\langle[u]_z\rangle\langle[c]_z\rangle\right]_y}_{\mathcal{T}_a} + \underbrace{W\left[\langle D\rangle\langle[u]'_z[c]'_z\rangle\right]_y}_{\mathcal{T}_b} + \underbrace{W\left[\langle D\rangle\left[\langle\tilde{u}\rangle\langle\tilde{c}\rangle\right]_z\right]_y}_{\mathcal{T}_c}\\ &\quad + \underbrace{W\left[\langle D\rangle\left[\langle\tilde{u}'\tilde{c}'\rangle\right]_z\right]_y}_{\mathcal{T}_d} + \underbrace{W\left[\langle D'[uc]'_z\rangle\right]_y}_{\mathcal{T}_e},\end{aligned} \qquad 8.$$

Table 1 Explanation of transport terms resulting from the decomposition of the cross-sectionally integrated and tidally averaged suspended particulate matter (SPM) transport shown in Equation 8

Symbol	Name	Process description
$\mathcal{T}_a$	Transport by averages	Down-estuary transport driven by river runoff
$\mathcal{T}_b$	Tidal covariance transport	E.g., up-estuary transport due to greater depth-mean SPM concentration during flood than during ebb; often referred to as tidal pumping
$\mathcal{T}_c$	Vertical covariance of tidal averages transport	Transport by estuarine exchange flow, with greater SPM concentrations near the bed, where residual flow is up-estuary
$\mathcal{T}_d$	Combined vertical and temporal covariance transport	E.g., SPM mixed higher up into the water during flood than during ebb by tidal straining (higher turbulence during flood than ebb resulting from destabilization of the water column)
$\mathcal{T}_e$	Temporal depth covariance transport	Water depth covariance with velocity (Stokes transport), SPM concentration, or both

where a prime denotes the deviation from a tidal average and a tilde denotes the deviation from a vertical mean (see details in **Supplemental Appendix 1**) and the expression $\langle D[uc]_z \rangle$ is the tidally averaged, depth-integrated SPM transport. Note that Equation 8 is exact only for constant depth or averaging in depth-proportional σ coordinates. **Table 1** explains the meaning of the cross-sectionally integrated, temporally averaged transport terms in Equation 8.

Supplemental Material

We would like to stress that the transport $\langle D[uc]_z \rangle$ typically has a distinct lateral structure and is affected by various processes. For example, the strength of estuarine circulation scales with the Simpson number, $Si \propto \langle D \rangle^2$ (Geyer et al. 2000, Burchard et al. 2011), so the estuarine circulation and associated landward SPM transport contribution to $\mathcal{T}_c$ tend to be strongest in the channel. The net river outflow and seaward component of the baroclinic exchange are stronger near the surface and more prominent on the shoals, leading to net seaward SPM transport. For example, in the Hudson River, SPM transports are landward in the channel and seaward on the shoals along the length of the salinity intrusion (Panuzio 1965, Ralston & Geyer 2009, Ralston et al. 2012). Bathymetry also creates lateral structure in bottom salinity fronts, and consequently tidal asymmetry in SPM concentration leading to net transport that is landward in the channel and seaward on the shoals (Geyer et al. 2001, Ralston et al. 2012).

4. SEDIMENT TRAPPING AT THE SALT INTRUSION LIMIT

ETM formation at the landward tip of the salt intrusion (for a description, see Section 2.1) can be quantitatively explained by considering a vertical exchange flow that exists in the salt wedge region but is absent in the tidal freshwater region. Here, we first explain sediment transport by exchange flow (vertical covariance, Section 4.1) and then illustrate its convergence at the salt intrusion limit (Section 4.2).

4.1. Sediment Transport by Vertical Covariance

To demonstrate the basic baroclinic mechanism of SPM trapping in estuaries caused by a subtle imbalance of seaward advective transport, $\mathcal{T}_a$, and landward exchange flow transport, $\mathcal{T}_c$, we next analyze results of one-dimensional water column models based on tidally averaged forcing and vertically constant longitudinal buoyancy gradients. Exchange flow with up-estuary flow near the bottom and down-estuarine flow near the surface driven by the estuarine density gradient is obtained by constant (Hansen & Rattray 1965, Ralston et al. 2008) and parabolic (Burchard

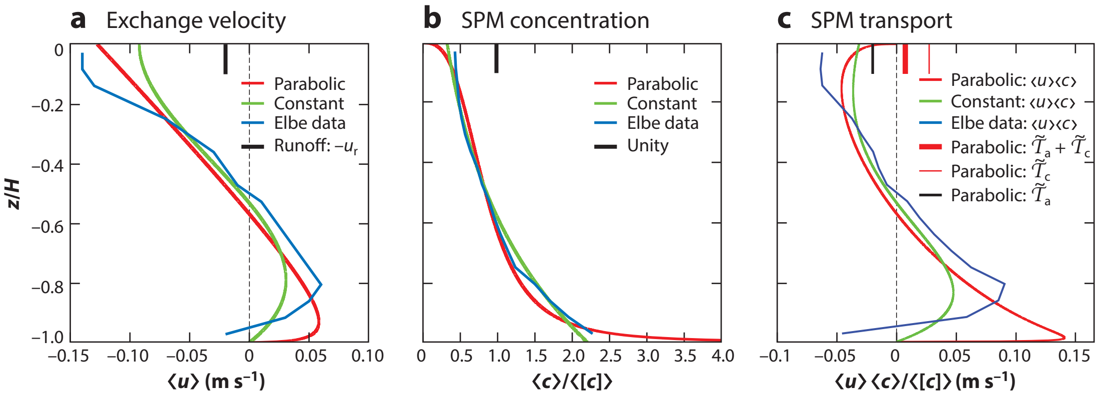

Figure 4

Profiles of (*a*) exchange flow velocity, (*b*) SPM concentration normalized by depth-mean SPM concentration, and (*c*) SPM transport components normalized by depth-mean SPM concentration. Depth-averaged values and transports ($\tilde{\mathcal{T}}_a = \mathcal{T}_a/\langle A\rangle$ and $\tilde{\mathcal{T}}_c = \mathcal{T}_c/\langle A\rangle$, shown only for parabolic eddy viscosity and diffusivity) are indicated by a thick vertical line at the top of each panel. All profiles are derived from analytical solutions and field observations. Red lines are solutions based on parabolic eddy viscosity and diffusivity, green lines are solutions based on constant eddy viscosity and diffusivity, and blue lines are field data from the Elbe estuary (from Kappenberg et al. 1995). For the analytical solutions, the dimensional parameters have been fitted to match the observations. Details are given in **Supplemental Appendix 2**. Abbreviation: SPM, suspended particulate matter.

Supplemental Material

& Hetland 2010) eddy viscosity (see **Figure 4*a***). For constant eddy diffusivity, SPM profiles are exponential, and for a parabolic eddy diffusivity, SPM profiles are similar to the Rouse (1939) profiles (**Figure 4*b***; for details, see **Supplemental Appendix 2**).

The SPM transport by averages (river runoff), $\mathcal{T}_a$, is directed seaward, and the transport caused by vertical covariance of tidal averages (exchange flow), $\mathcal{T}_c$, is directed landward, such that in this case the sum of both is close to zero (see **Figure 4*c***). Note that the vertical covariance converges to zero for vanishing settling velocity because in that case c' is vanishing as well. Observations taken in the Elbe estuary are quantitatively comparable to the analytical solutions because similar external parameters have been chosen (see **Figure 4*c***).

Processes other than gravitational circulation can contribute to the exchange flow $\langle\tilde{u}\rangle$ (MacCready & Geyer 2010, Geyer & MacCready 2014). The eddy viscosity and vertical shear covariance (see Dijkstra et al. 2017b) has the potential to substantially increase the exchange flow (Burchard et al. 2011). As proposed by Jay & Musiak (1994), one important contributor to the eddy viscosity and vertical shear covariance is the tidal straining (Simpson et al. 1990) that occurs when the flood eddy viscosity is greater than the ebb eddy viscosity. Lateral circulation (Lerczak & Geyer 2004), wind straining (Scully et al. 2005), estuarine convergence (Ianniello 1979, Burchard et al. 2014), and Coriolis acceleration (Huijts et al. 2009) have the potential to increase the exchange flow intensity. In addition, the tidally averaged SPM concentration profile $\langle c\rangle$ depends on numerous processes, such as hindered settling at high concentrations of cohesive SPM (Winterwerp 2001), net exchange with the bed (Burchard et al. 2013), or suppression of vertical turbulent SPM transports by vertical stratification (Scully & Friedrichs 2003). Because the exchange flow is also increased by vertical stratification, the latter process increases the vertical covariance between tidally averaged velocity and SPM concentration, leading to an enhanced up-estuary SPM transport (Geyer 1993, Burchard & Baumert 1998).

4.2. Convergence at the Salt Intrusion Limit

The trapping mechanism shown in **Figure 2** can be reproduced by using the mathematical framework presented in Section 4.1 along with parabolic profiles of eddy viscosity and diffusivity. It results from an idealization of the cross-sectionally integrated, tidally averaged sediment concentration described by Equation 6, assuming negligible temporal and spatial variations of the cross-sectional area A (including the rigid-lid assumption, absence of lateral net sediment transports, and source and sink terms) and negligible lateral variations in depth, velocity, and sediment concentration, and applying a constant runoff velocity with a constant background SPM concentration (for details, see **Supplemental Appendix 2**). The estuarine salinity gradient is represented by a Gaussian-shaped longitudinal salinity gradient (**Figure 5*a***). The balance of SPM transport is between downstream transport with the mean flow ($\mathcal{T}_a$) and upstream transport with the exchange flow ($\mathcal{T}_c$) (see **Figure 5*b***). Landward of the location of the salinity gradient (salt wedge), the resulting transport ($\mathcal{T}_a + \mathcal{T}_c$ in **Figure 5*b***) is downstream with the river flow, but in the core of the salt wedge it is balanced by positive SPM transport. Landward from the maximum positive SPM transport, the SPM transport is convergent, leading to SPM trapping and the evolution of an ETM, which converges after a few months to maximum concentrations of 0.55 kg m^{-2} (**Figure 5*c***). Because of the asymmetry of the forcing, the resulting ETM is asymmetric as well,

Supplemental Material

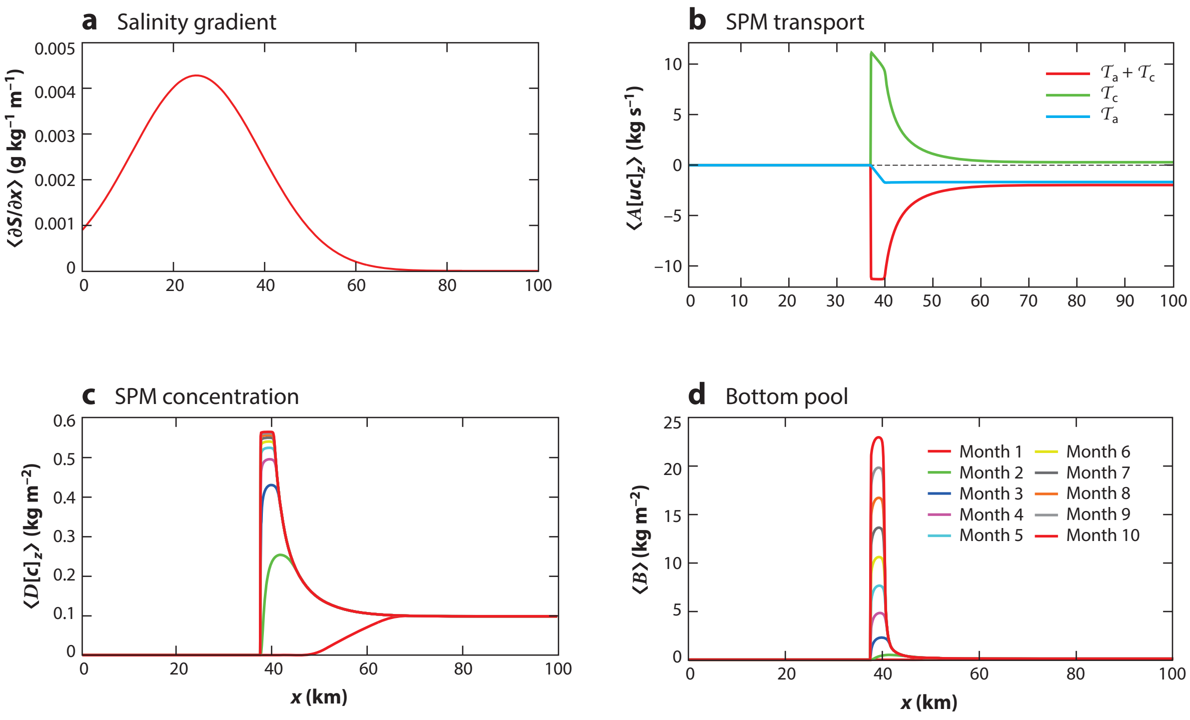

Figure 5

Semianalytical solutions of ETM formation at the salt intrusion limit over 10 months, based on parabolic eddy viscosity and diffusivity profiles, assuming a width of 500 m and a runoff velocity of 0.04 m s^{-1} (for details, see **Supplemental Appendix 1**). (*a*) Salinity gradient $\partial S/\partial x$. (*b*) Cross-sectionally integrated SPM transport $\langle A[uc]_z\rangle$ and its decomposition into $\mathcal{T}_a$, $\mathcal{T}_c$, and their sum after 10 months. (*c*) Depth-integrated SPM concentration in the water column $\langle D[c]_z\rangle$. (*d*) The bottom pool $\langle B\rangle$. Abbreviations: ETM, estuarine turbidity maximum; SPM, suspended particulate matter.

and because of the stationary SPM transport convergence, the ETM becomes oversaturated, such that the bottom pool grows steadily (**Figure 5*d***).

5. SEDIMENT TRAPPING IN THE FRESHWATER REGION

In tidally energetic estuaries, ETMs also form in the freshwater zone (Section 2.2). In the absence of salinity gradients, tidal forcing is the only way to transport SPM upstream against the residual river runoff. Here, we first explain sediment transport caused by temporal covariance (Section 5.1) and then discuss quantitatively how the convergence of such transports results in the formation of freshwater ETMs (Section 5.2).

5.1. Sediment Transport by Temporal Covariance

Apart from the transport contributions $\mathcal{T}_a$ and $\mathcal{T}_c$ described in Section 3.3, all contributions to Equation 8 result from temporal covariances. Well-known contributions are related to tidal velocity asymmetry and temporal and spatial settling lag (see de Swart & Zimmerman 2009, Friedrichs 2011; for details, see **Supplemental Appendix 3**). Tidal velocity asymmetry results in a residual SPM transport in the direction of the peak current. Local inertia in Equation 1 can result in net transport caused by tidal duration asymmetry, also known as transport caused by temporal settling lag (Groen 1967, Dronkers 1986). This net transport contribution is in the direction of the flood (ebb) current if the maximal flood (ebb) current is followed by the longest slack tide.

Supplemental Material

Spatial variations in SPM concentration can also result in net transport (Postma 1954, Van Straaten & Kuenen 1958), a mechanism referred to as spatial settling lag. The resulting residual SPM transport is in the direction of decreasing SPM concentration. This SPM gradient can result from many different mechanisms (Friedrichs 2011).

Internal asymmetries in eddy diffusivity and settling velocity may contribute to $\mathcal{T}_d$ even for symmetric resuspension (Scully & Friedrichs 2007). During flood tides, high SPM concentrations ($\tilde{c}' > 0$) might be mixed higher up in the water column, coinciding with flood velocities ($\tilde{u}' > 0$), and during ebb tides ($\tilde{u}' < 0$), SPM concentrations might be mixed lower in the water column ($\tilde{c}' < 0$), leading to $\langle \tilde{u}'\tilde{c}' \rangle > 0$. A similar effect results from asymmetric settling velocity: Greater turbulence during flood may reduce the mean floc diameter of cohesive SPM and thus the settling velocity (see Section 8.1), such that near-surface SPM concentrations may increase during flood (Scully & Friedrichs 2007). When resuspension is limited, near-bed SPM concentration may be reduced ($\tilde{c}' < 0$) during flood such that the covariance $\langle \tilde{u}'\tilde{c}' \rangle$ has a negative contribution (Burchard et al. 2013).

The component $\mathcal{T}_e$ contains SPM transport caused by temporal covariance with water depth, which is relevant when the tidal amplitude is large compared with the mean water depth. A further decomposition of $\mathcal{T}_e$ (see Díez-Minguito et al. 2014) shows that it also includes the covariance between current velocity and water depth, commonly referred to as the Stokes transport (Zimmerman 1979).

5.2. Convergence in the Freshwater Zone

To illustrate the ETM formation in the freshwater zone, we consider only the SPM transport related to velocity amplitude asymmetry, using a similar approach as adopted in Section 4.2. The model description and solution method have been described by Dijkstra et al. (2017a) and implemented in the free software package iFlow. The estuary is exponentially converging, and there is no sediment input from the landward side. Initially, there is almost no SPM available in

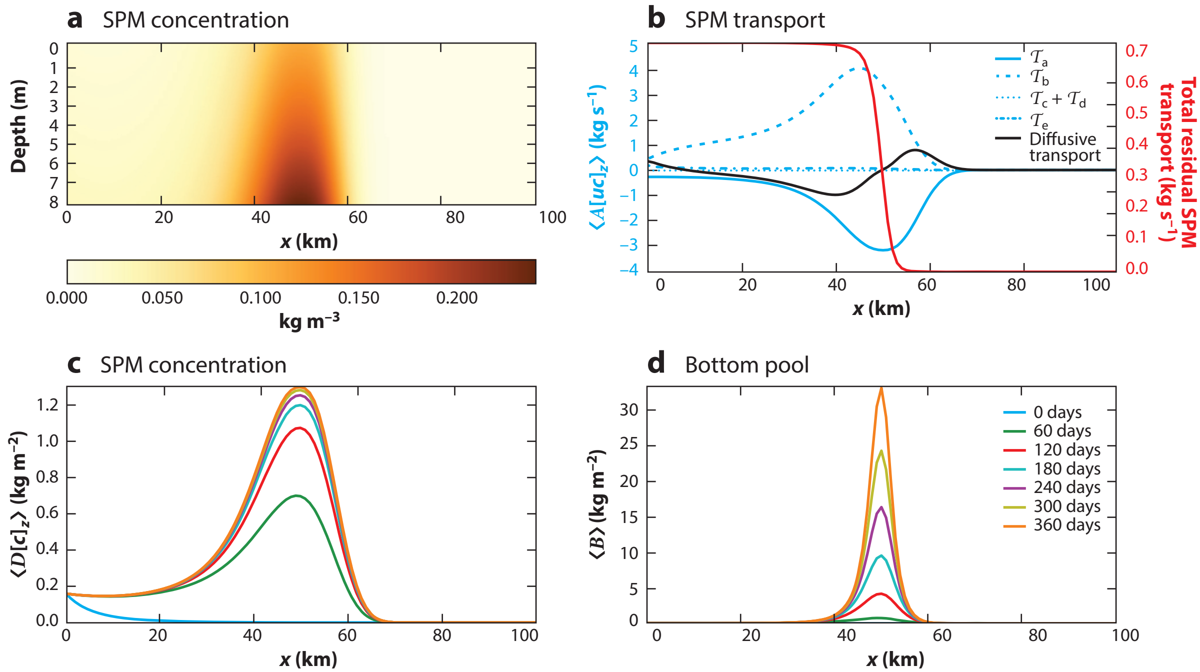

Figure 6

SPM transport and trapping in the freshwater zone caused by tidal velocity asymmetry. The parameter values used are given in **Supplemental Appendix 3**. (*a*) Tidally averaged SPM concentration after 360 days. (*b*) Total tidally averaged SPM transport (*red line*) and different components (*blue lines*) after 360 days. (*c*) Temporal evolution of the depth-integrated residual SPM concentration for the first 360 days. (*d*) Temporal evolution of the bottom pool for the first 360 days. Abbreviation: SPM, suspended particulate matter.

Supplemental Material

the estuary (see **Figure 6*c***). **Figure 6*a*** shows the resulting tidally averaged SPM concentration after 360 days, with a clear ETM at approximately 50 km from the seaward side. The maximum concentration is approximately 240 mg L^{-1}. **Figure 6*b*** shows the corresponding residual SPM transport, indicating a constant SPM transport from the seaward side toward the trapping region, where the SPM deposits. Landward of the ETM, there is no residual SPM transport. **Figure 6*b*** also shows the different SPM transport contributions (see Equation 8). SPM is exported mainly because of the advection of tidally averaged concentration by the river flow ($\mathcal{T}_a$), whereas import is the result of the asymmetry between ebb and flood velocities ($\mathcal{T}_b$). In **Figure 6*c*,*d***, the temporal evolutions of the total amount of SPM in the water column and the bottom pool are shown for the first 360 days. Changes in SPM concentration in the water column decrease over time, indicating that the SPM distribution is approaching an equilibrium. The amount of SPM in the bottom pool, however, still increases.

This scenario and those in **Supplemental Appendix 3** elucidate the role of various trapping mechanisms in the freshwater zone. These and other trapping mechanisms usually work simultaneously, and assessing which mechanism is essential for trapping in a specific estuary requires a detailed analysis of the SPM transport contributions.

6. SEDIMENT TRAPPING IN EXAMPLE ESTUARIES

Here, we demonstrate the decomposition of the cross-sectionally integrated SPM transports (Equation 8) and their convergence in model simulations first for an idealized convergent

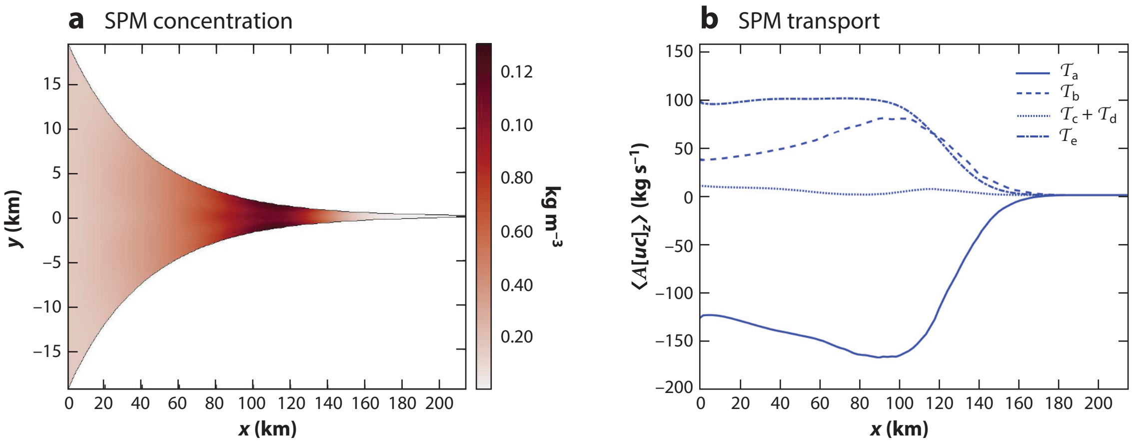

Figure 7

An idealized example estuary: (*a*) an ETM in morphodynamic equilibrium and (*b*) the corresponding residual cross-sectionally integrated sediment transport contributions. Abbreviations: ETM, estuarine turbidity maximum; SPM, suspended particulate matter.

estuary to analyze specific processes leading to a freshwater ETM (Section 6.1) and then for a complex and realistic model of the Hudson River estuary to closely reproduce and understand the observed dynamics (Section 6.2).

6.1. Idealized Convergent Estuary

Our idealized estuary uses the dimensions of the Delaware River estuary (for details, see Wei 2017): a length of 215 km, a width at the mouth of 39 km, and an exponential convergence length of 42 km. The bathymetry consists of a single channel in the center of the estuary. The water motion at the seaward side is forced by prescribed M_2 and M_4 tidal elevation amplitudes of 75 cm and 1.2 cm, respectively; at the landward side, a river discharge of 288 $m^3\ s^{-1}$ is prescribed. Assuming the system to be in morphodynamic equilibrium, an ETM is located approximately 100 km from the entrance (**Figure 7*a***). From **Figure 7*b***, it follows that there is an approximate balance between the import associated with $\mathcal{T}_b$ and $\mathcal{T}_e$ and the export $\mathcal{T}_a$. These contributions can be further decomposed into two-dimensional transports associated with different transport mechanisms (for details, see Kumar et al. 2017, Wei 2017).

6.2. Hudson River Estuary

A realistic simulation of the Hudson River estuary provides an example of the SPM transport decomposition that includes natural variability in forcing and bathymetry. The simulation analyzed here is from the spring freshet of 2014 (Ralston & Geyer 2017). SPM transport varies temporally with river discharge and spatially with salinity intrusion (**Figure 8**). Transport is strongly seaward with each of the discharge events, extending to near the mouth. During lower discharge and neap tides, the salinity intrusion extends farther landward (Ralston et al. 2008), and near the limit of salinity intrusion, the transport becomes less seaward or even landward. The transport by averages $\mathcal{T}_a$ (**Figure 8*b***) corresponds with river influence except during brief periods of landward transport caused by coastal water level fluctuations. The vertical covariance of the tidally averaged transport $\mathcal{T}_c$ (**Figure 8*d***) is primarily landward, particularly within the salinity intrusion, where the estuarine

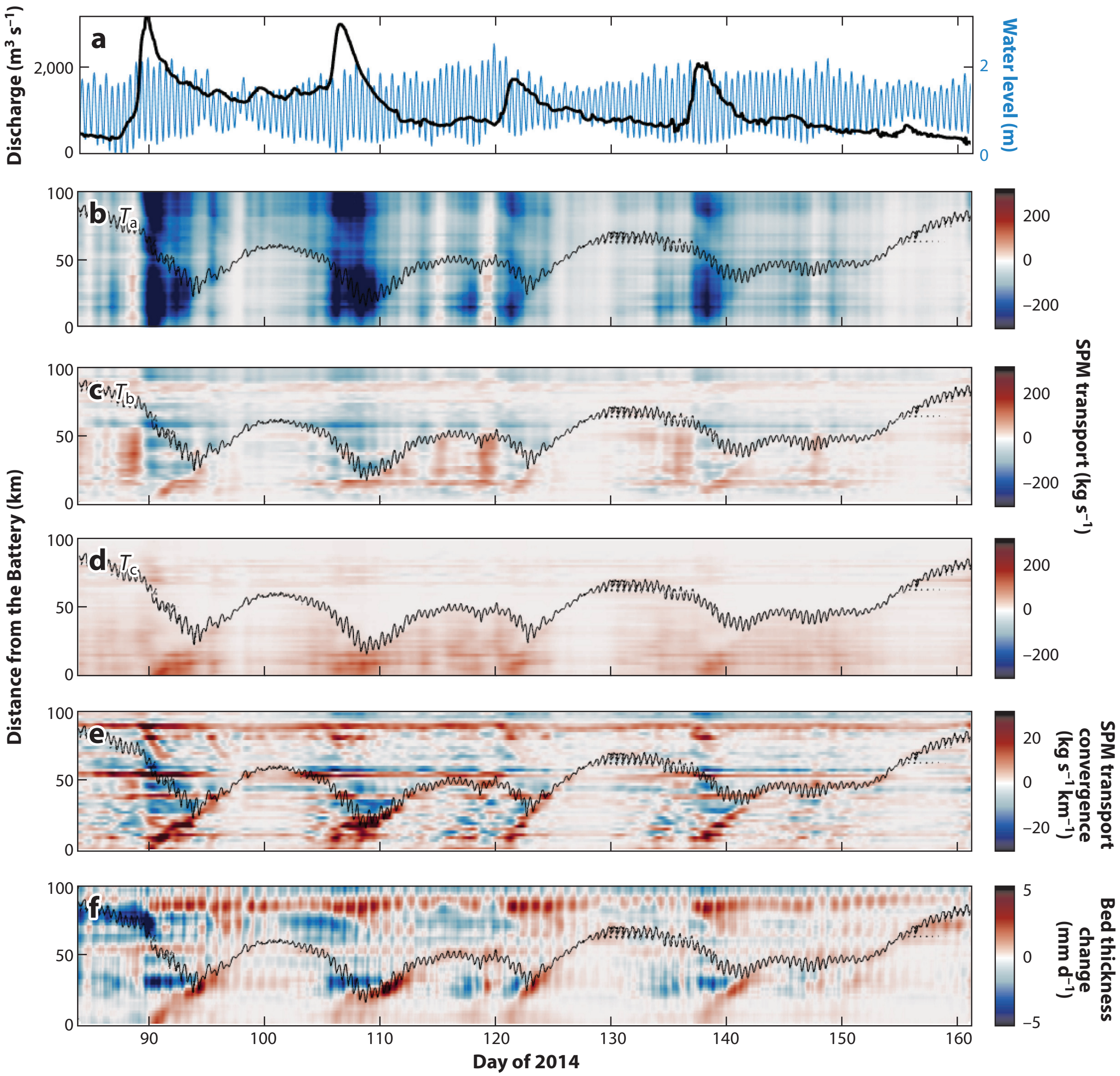

Figure 8

SPM transport decomposition for the Hudson River estuary during the spring freshet of 2014 (model results; see Ralston & Geyer 2017). The black contours in each panel are the 1 g kg^{-1} bottom salinity isohalines. (*a*) Discharge (*left axis*) and water level (*right axis*). (*b*) Transport by averages, $\mathcal{T}_a$, as a function of distance from the river mouth and day of the year. (*c*) Transport by tidal covariance, $\mathcal{T}_b$, as a function of distance from the river mouth and day of the year. (*d*) Transport by vertical covariance of tidal averages, $\mathcal{T}_c$, as a function of distance from the river mouth and day of the year. (*e*) Along-estuary SPM transport convergence (*red*) or divergence (*blue*). (*f*) Rate of change in bed thickness caused by net deposition (*red*) or erosion (*blue*). Abbreviation: SPM, suspended particulate matter.

circulation moves near-bed SPM landward. The tidal covariance transport $\mathcal{T}_b$ (**Figure 8*c***) also depends strongly on the salinity intrusion. In the tidal fresh region, the tidal covariance transport $\mathcal{T}_b$ is mostly seaward, likely because there are stronger velocities and more SPM during ebbs than during floods because of the river discharge. Within the salinity intrusion, $\mathcal{T}_b$ is landward because of the greater SPM concentrations during flood tides in salinity fronts at topographic transitions (Geyer et al. 2001, Ralston et al. 2012). Both the tidal covariance transport $\mathcal{T}_b$ and vertical covariance transport $\mathcal{T}_c$ are strongest in the lower estuary (10–30 km in **Figure 8*c*,*d***), where salinity fronts occur for most discharge conditions.

SPM concentrations are greater in the lower estuary, particularly during spring tides and discharge events. A zone of along-estuary convergence propagates landward during neap tides with the salinity intrusion (**Figure 8*e***). Corresponding with this convergence is a depositional region that increases the supply of bed sediment for resuspension, most notably in the lower ETM (∼20 km in **Figures 1** and **8*f***). A second convergence and deposition zone at approximately 55 km is spatially locked and associated with frontal trapping at a constriction (Ralston et al. 2012) (**Figure 1**). At approximately 90 km, a region that is fresh for most discharges has convergence, deposition, and locally elevated SPM (as in **Figure 1**) downstream from a lateral expansion.

7. TIMESCALES

SPM trapping depends on forcing that varies at multiple timescales. Tidal amplitude varies with the spring-neap cycle and affects resuspension, stratification, and estuarine circulation. River discharge varies at event and seasonal timescales and affects the advection of salinity and SPM as well as the SPM supply from the watershed. Bathymetry is relatively static at fortnightly to annual timescales, but over decades to centuries, geomorphic change and anthropogenic modification affect tidal velocities and estuarine circulation. Because SPM trapping depends on the forcing variability as well as the response of the estuary, ETMs are rarely static in location or intensity.

7.1. Spring-Neap Cycle

The spring-neap cycle is often the dominant timescale for SPM, more so than seasonal variation with river discharge and SPM supply. Increased velocities during spring tides enhance bed stress and reduce stratification, leading to greater SPM concentrations. The spring-neap cycle dominates the SPM variance in mesotidal, partially mixed estuaries like those of San Francisco Bay (Schoellhamer 2002), the Hudson (Traykovski et al. 2004), and the Columbia (Fain et al. 2001, Hudson et al. 2017) and in macrotidal, well-mixed estuaries like those of the Gironde (Doxaran et al. 2009) and the Seine (Le Hir et al. 2001). The inventory of the mobile pool can be much greater than the annual input from the watershed, so SPM is limited by the tidal energy for resuspension rather than by the fluvial supply (Schoellhamer 2011).

In addition to resuspension, tidal amplitude affects SPM trapping. Increased velocities enhance landward transport by tidal pumping (tidal covariance), as in the Thames (Mitchell et al. 2012), the Changjiang (Song et al. 2013), and the Humber (Uncles et al. 2006). By contrast, spring tides reduce the trapping by estuarine circulation. In systems dominated by this mechanism, SPM transport is landward during neap tides as mixing decreases and salinity expands landward, and export increases during spring tides when the salinity shifts seaward (Schoellhamer 2000, Fain et al. 2001, Ralston & Geyer 2009). Owing to the spring-neap variation in resuspension and export, SPM accumulates in estuaries during neaps and is lost during spring tides (Allen et al. 1980, Geyer 1993).

7.2. Event and Seasonal Discharge Variability

River discharge can increase by an order of magnitude over several days, and the variation from spring freshet to summer low discharge can be even greater. Discharge alters the location of the salinity intrusion and thus of SPM trapping, and the river velocity can limit the landward propagation of tides and shift the tidal fresh ETM. SPM input from the watershed also varies strongly with discharge (Nash 1994). The fate of SPM delivered during discharge events depends on the timing with respect to the spring-neap cycle (Ralston & Geyer 2009) and the antecedent discharge conditions (Sanford et al. 2001, Ralston et al. 2013) because both affect the salinity distribution and therefore trapping.

Seasonal discharge variation controls the location of trapping in many estuaries, shifting seaward during higher discharge with the salinity intrusion, as in San Francisco Bay (Sanford et al. 2001), the Weser (Kappenberg & Grabemann 2001), and the Hudson (Ralston et al. 2012). In macrotidal estuaries, increased discharge can reduce flood dominance and shift SPM convergence seaward (Mitchell et al. 2012). In the Humber and the Gironde, ETMs move from the salinity limit during high discharge to the tidal fresh region during lower discharge (Allen et al. 1980, Uncles et al. 2006). Along-estuary shifts in ETM position are not immediate but lag the river forcing by weeks to months (Allen et al. 1980, Wellershaus 1981). With increasing discharge, SPM accumulated in the mobile bottom pool is eroded over many tidal cycles, and SPM concentrations lag the seaward shift in salinity (Sommerfield & Wong 2011, Mitchell et al. 2012). During decreasing discharge, landward movement of the ETM occurs over several months as the pool of erodible sediment steadily increases (Uncles et al. 2006, Jalón-Rojas et al. 2016).

8. ANTHROPOGENIC AND GEOMORPHIC CHANGE

Over decades to centuries, estuaries generally accrete at rates similar to local sea level rise, given sufficient sediment supply (Meade 1969, Klingbeil & Sommerfield 2005). Alterations to sediment supply by dam building or land use changes occur more suddenly, but the response time for SPM can be long. In San Francisco Bay, dam construction reduced the sediment supply in the mid-1900s, but the SPM concentration did not decrease for decades with the gradual depletion of accumulated sediment (Schoellhamer 2011). In the Yangtze, the response of the ETM was modest compared with the supply reduction by dams because the mobile bottom pool of SPM was an order of magnitude larger than the annual input (Song et al. 2013). The mass in the mobile pool must be much greater than the average annual input to accommodate the wide variability in supply with discharge (Schoellhamer 2011), even though at tidal timescales the mass in suspension corresponds to a small fraction of the total (Wellershaus 1981).

Contaminant histories reflect the long timescales of the mobile pool (Menon et al. 1998, Schoellhamer et al. 2007). For example, mercury released in the 1970s in the Penobscot River now has a nearly uniform concentration in mobile SPM and a residence time of approximately 25 years (Geyer & Ralston 2018). In the Passaic River, dioxin accumulated in the estuary despite being released near the mouth because channel dredging greatly increased the trapping efficiency (Chant et al. 2011). Dredging has increased the rates of deposition in many estuaries (Meade 1969, Nitsche et al. 2010, Song et al. 2013, de Jonge et al. 2014). Increased trapping with dredging increases the size of the mobile pool, thereby increasing the residence times of SPM and contaminants. Quantifying the mobile pool remains a major challenge but is critical to understanding the cycling of SPM and associated organic matter and contaminants.

8.1. Hyperturbid Estuaries

In recent decades, several European estuaries have experienced significant increases in tidal range and SPM concentrations, evolving from relatively low-SPM estuaries into hyperturbid estuaries (i.e., systems with strongly elevated SPM concentrations compared with past concentrations). Examples include the Loire River (Jalón-Rojas et al. 2016) and the Ems estuary (Talke et al. 2009, Schuttelaars et al. 2013, de Jonge et al. 2014). In the Ems, the maximum surface concentration increased from approximately 200 mg L^{-1} in the 1950s to approximately 1 g L^{-1} in 2006, the location of the ETM shifted landward from the limit of saltwater intrusion into the freshwater zone (figure 3 in de Jonge et al. 2014 and **Figure 1**), and thick layers of fluid mud formed (Van Leussen 1994, Winterwerp et al. 2017).

Winterwerp (2011) and Winterwerp & Wang (2013) proposed a conceptual model to explain this evolution. As a first step in their model, tidal channels are deepened (usually for shipping purposes) and intertidal areas are removed, resulting in tidal amplification and net transport of marine SPM into the freshwater zone. River deepening also reduces mean outflow velocities and seaward SPM transport, allowing the formation of a freshwater ETM (Winterwerp 2011). The deepening and topping off of bedforms and stratification effects from the accumulation of fine SPM in the water column (Vanoni 1946, Soulsby & Wainwright 1987) result in hydraulic drag reduction, allowing further tidal amplification, net import of SPM, and so on. Owing to this feedback process, the estuary becomes hyperturbid, a highly stable configuration with very high suspended SPM concentrations and pools of fluid mud at the bed. Winterwerp (2011) calls this state an alternative steady state and refers to the evolution from a relatively low-concentration estuary to a hyperturbid one as a regime shift. The timescale necessary for this regime shift can be long (years to decades) because the accumulation of fines to reduce the hydraulic drag takes time and is influenced by river discharge events that tend to flush fine SPM seaward and by trapping of fines on tidal flats and side embayments of the estuary.

Reproducing this conceptual mechanism in process-based models requires taking into account the feedbacks between the water motion and SPM and the influence of high SPM on the settling velocity. SPM-induced stratification can damp turbulence and modify the velocity shear, vertical mixing, and bottom roughness, as observed in laboratory environments (Einstein & Chien 1955) and turbid estuaries (Wolanski et al. 1988, Trowbridge et al. 1994) and modeled by Barenblatt (1953), Winterwerp (2001), Wang (2002), and Wang et al. (2005). Temporal variability in vertical mixing can generate residual circulation and overtides (Jay & Musiak 1996, Dijkstra et al. 2017b), modifying SPM transport, whereas temporal variability in eddy diffusivity modifies SPM transport by the mechanism discussed by Scully & Friedrichs (2003).

High SPM concentrations can also modify the longitudinal density gradient, as in the Ems estuary (**Figure 1**). The SPM concentration gradient affects the density-driven circulation and hence the residual SPM transport. In the Ems, SPM gradients enhance residual circulation upstream of the ETM and reduce residual circulation downstream of the ETM (Talke et al. 2009).

The dependence of settling velocity on SPM concentration through hindered settling and flocculation also becomes important. Flocculation is a reversible process that results from simultaneous aggregation and floc breakup processes (Van Olphen 1977) and is dominated by turbulent effects in estuaries (Winterwerp & van Kesteren 2004). Van Leussen (1994) included these effects heuristically by relating the settling velocity to the shear rate parameter. Winterwerp (2002) derived a conservation equation for the number concentration of flocs of cohesive SPM combined with a relation between floc size and settling velocity. At higher concentrations, flocs start to interact and modify the flow, thus hindering each other when settling (Scott 1984, Winterwerp & van Kesteren 2004). Hindered settling is usually modeled with the formula by Richardson & Zaki (1954); an alternative formulation was proposed by Dankers & Winterwerp (2007).

Le Hir et al. (2001), Winterwerp (2001), and Winterwerp et al. (2006) developed one-dimensional point models containing some of the processes mentioned above in order to study the temporal dynamics of SPM stratification and the formation of lutoclines in a water column. These water column models were able to qualitatively reproduce the observed behavior of SPM stratification in estuaries by including SPM-induced turbulence damping and hindered settling effects.

One of the current challenges is to extend beyond the one-dimensional models above while resolving the flow-turbidity feedbacks, hindered settling, and flocculation processes accurately enough. In addition, accurately describing the bottom boundary conditions, especially in the presence of fluid mud, remains challenging.

9. FUTURE ISSUES

This review has shown that sediment trapping in estuaries is a result of convergent SPM transport, which is well known to occur at the limit of the salinity intrusion, where landward SPM transport by the estuarine circulation meets seaward transport from the river outflow, leading to an ETM. ETMs also occur in the tidal freshwater regions, where landward transport by tidal processes is reduced near the limit of propagation. Detailed examination of ETMs shows that lateral and along-estuary bathymetric gradients can induce similar SPM trapping processes at multiple locations within an estuary, leading to significant spatial and temporal variation in the location and intensity of ETMs. In the example from the Hudson River estuary (Section 6.2), the mechanisms of estuarine circulation and tidal pumping are present, and the spatial variability with bathymetry and temporal variability with river discharge and tidal amplitude are so important that the mechanism related to the salt wedge is almost hidden. Some of those trapping processes are stationary, because they are driven by topographic convergence, and some of them move with the salinity intrusion.

It is evident from observations (Wellershaus 1981) and mathematical analysis (Sections 4.2 and 5.2) that the interaction with the bed sediment is decisive for the development of an ETM, because the SPM capacity of the water column is limited and any further convergent SPM transport beyond that limit would lead to an increasing bottom sediment pool. Although the locations of the convergence zones are highly variable in time (Section 6.2), the bottom pool acts as a restoring force for the ETM location. This was first reported almost 30 years ago (Lang et al. 1989), but the involved processes and timescales are not well constrained.

SPM in estuaries is composed of marine and fluvial material, and the relative importance of landward and seaward sediment inputs varies widely among estuaries. Although it is obvious that the fluvial material enters the estuary through the river runoff, the transport of the marine material toward the mouth varies with the estuary and remains difficult to quantify. A general understanding of SPM pathways and transport processes from the shelf sea into the estuary is still missing.

Several European estuaries that have been intensively dredged and narrowed turned into hyperturbid estuaries (Section 8.1), a transition that causes substantial ecological and economic problems. Other heavily engineered estuaries have not experienced this transition but might be close to it (Winterwerp et al. 2013). The processes and parameters that determine the transition to hyperturbid states of estuaries are not yet sufficiently understood.

Reaching the goal of classifying estuaries in terms of their ETM dynamics [as Geyer & MacCready (2014) accomplished for the estuarine hydrodynamics] will require more fundamental research in estuarine SPM dynamics.

In summary, the following research challenges remain:

- How can the relative importance of tidal and topographic trapping be assessed in comparison with trapping at the landward limit of the salt wedge, and how much do these processes interact nonlinearly?
- How do lateral hydrodynamic processes contribute to longitudinal convergence in SPM transports?
- What are the adjustment timescales of SPM dynamics and ETM formation in response to changing hydrodynamic conditions?

- How do the fast dynamics of SPM in the water column and the slow dynamics of the bottom pool interact to determine ETM locations and variability, and what processes govern the dynamics of the mobile bottom pool?
- What are the fractions of fluvial and marine SPM classes in ETMs, and what are the transport mechanisms to bring marine SPM from the shelf sea into the estuary?
- What processes trigger the transition from normal to hyperturbid estuaries, and how much does the transition depend on direct human invention such as deepening or narrowing?
- How can estuaries be classified in terms of their ETM dynamics?

DISCLOSURE STATEMENT

The authors are not aware of any affiliations, memberships, funding, or financial holdings that might be perceived as affecting the objectivity of this review.

ACKNOWLEDGMENTS

H.B. was supported by the Morphodynamic Response of the Wadden Sea to Climate Change (MOREWACC) project funded by the German Research Foundation as BU 1199/21-1 under the umbrella of Priority Program SPP 1889 on Regional Sea Level Change and Society. D.K.R. was supported by the National Science Foundation (OCE #1325136). The authors are grateful to Stefan Talke and David Jay for reviewing an early version of this article and to Jens Kappenberg for providing the Elbe data for **Figures 1*a*** and **4**.

LITERATURE CITED

Allen GP, Salomon JC, Bassoullet P, Du Penhoat Y, De Grandpre C. 1980. Effects of tides on mixing and suspended sediment transport in macrotidal estuaries. *Sediment. Geol.* 26:69–90

Ariathurai CR. 1974. *A finite element model of cohesive sediment transportation*. PhD Thesis, Univ. Calif., Davis

Barenblatt GI. 1953. On the motion of suspended particles in a turbulent stream. *Prikl. Mat. Mekhanica* 17:261–74

Becherer J, Flöser G, Umlauf L, Burchard H. 2016. Estuarine circulation versus tidal pumping: sediment transport in a well-mixed tidal inlet. *J. Geophys. Res.* 121:6251–70

Brenon I, Le Hir P. 1999. Modelling the turbidity maximum in the Seine estuary (France): identification of formation processes. *Estuar. Coast. Shelf Sci.* 49:525–44

Burchard H, Baumert H. 1998. The formation of estuarine turbidity maxima due to density effects in the salt wedge. A hydrodynamic process study. *J. Phys. Oceanogr.* 28:309–21

Burchard H, Hetland RD. 2010. Quantifying the contributions of tidal straining and gravitational circulation to residual circulation in periodically stratified tidal estuaries. *J. Phys. Oceanogr.* 40:1243–62

Burchard H, Hetland RD, Schulz E, Schuttelaars HM. 2011. Drivers of residual circulation in tidally energetic estuaries: straight and irrotational estuaries with parabolic cross-section. *J. Phys. Oceanogr.* 41:548–70

Burchard H, Schulz E, Schuttelaars HM. 2014. Impact of estuarine convergence on residual circulation in tidally energetic estuaries and inlets. *Geophys. Res. Lett.* 41:913–19

Burchard H, Schuttelaars HM, Geyer WR. 2013. Residual sediment fluxes in weakly-to-periodically stratified estuaries and tidal inlets. *J. Phys. Oceanogr.* 43:1841–61

Cerco CF, Kim SC, Noel MR. 2013. Management modeling of suspended solids in the Chesapeake Bay, USA. *Estuar. Coast. Shelf Sci.* 116:87–98

Chant RJ, Fugate D, Garvey E. 2011. The shaping of an estuarine superfund site: roles of evolving dynamics and geomorphology. *Estuaries Coasts* 34:90–105

Chen SN, Sanford LP. 2009. Axial wind effects on stratification and longitudinal salt transport in an idealized, partially mixed estuary. *J. Phys. Oceangr.* 39:1905–20

Chernetsky AS, Schuttelaars HM, Talke SA. 2010. The effect of tidal asymmetry and temporal settling lag on sediment trapping in tidal estuaries. *Ocean Dyn*. 60:1219–41

Dankers P, Winterwerp J. 2007. Hindered settling of mud flocs: theory and validation. *Cont. Shelf Res.* 27:1893–907

de Jonge VN, Schuttelaars HM, van Beusekom JE, Talke SA, de Swart HE. 2014. The influence of channel deepening on estuarine turbidity levels and dynamics, as exemplified by the Ems estuary. *Estuar. Coast. Shelf Sci.* 139:46–59

de Swart HE, Zimmerman JTF. 2009. Morphodynamics of tidal inlet systems. *Annu. Rev. Fluid Mech.* 41:203–29

Díez-Minguito M, Baquerizo A, de Swart HE, Losada MA. 2014. Structure of the turbidity field in the Guadalquivir estuary: analysis of observations and a box model approach. *J. Geophys. Res.* 119:7190–204

Dijkstra YM, Brouwer RL, Schuttelaars HM, Schramkowski GP. 2017a. The iFlow modelling framework v2.4: a modular idealized process-based model for flow and transport in estuaries. *Geosci. Model Dev.* 10:2691–713

Dijkstra YM, Schuttelaars HM, Burchard H. 2017b. Generation of exchange flows in estuaries by tidal and gravitational eddy viscosity–shear covariance (ESCO). *J. Geophys. Res.* 122:4217–37

Doxaran D, Froidefond JM, Castaing P, Babin M. 2009. Dynamics of the turbidity maximum zone in a macrotidal estuary (the Gironde, France): observations from field and MODIS satellite data. *Estuar. Coast. Shelf Sci.* 81:321–32

Dronkers J. 1986. Tide-induced residual transport of fine sediment. In *Physics of Shallow Estuaries and Bays*, ed. J van de Kreeke, J Dronkers, pp. 228–44. Berlin: Springer

Dyer KR. 1988. Fine sediment particle transport in estuaries. In *Physical Processes in Estuaries*, ed. J Dronkers, W van Leussen, pp. 295–310. Berlin: Springer

Dyer KR. 1997. *Estuaries: A Physical Introduction*. Chichester, UK: Wiley & Sons

Einstein HA, Chien N. 1955. *Effects of Heavy Sediment Concentration Near the Bed on Velocity and Sediment Distribution*. Berkeley: Univ. Calif., Inst. Eng. Res.

Etcheber H, Taillez A, Abril G, Garnier J, Servais P, et al. 2007. Particulate organic carbon in the estuarine turbidity maxima of the Gironde, Loire and Seine estuaries: origin and lability. *Hydrobiologia* 588:245–59

Fain AMV, Jay DA, Wilson DJ, Orton PM, Baptista AM. 2001. Seasonal and tidal monthly patterns of particulate matter dynamics in the Columbia River estuary. *Estuaries Coasts* 24:770–86

Festa JF, Hansen DV. 1978. Turbidity maxima in partially mixed estuaries: a two-dimensional numerical model. *Estuar. Coast. Mar. Sci.* 7:347–59

Fischer H. 1972. Mass transport mechanisms in partially stratified estuaries. *J. Fluid Mech.* 53:671–87

Friedrichs CT. 2011. Tidal flat morphodynamics: a synthesis. In *Treatise on Estuarine and Coastal Science*, ed. E Wolanski, D McLusky, pp. 137–70. Waltham, MA: Academic

Friedrichs CT, Armbrust BD, de Swart HE. 1998. Hydrodynamics and equilibrium sediment dynamics of shallow, funnel-shaped tidal estuaries. In *Physics of Estuaries and Coastal Seas: Proceedings of the 8th International Biennial Conference on Physics of Estuaries and Coastal Seas*, ed. J Dronkers, MBAM Scheffers, pp. 315–27. Rotterdam, Neth.: Balkema

Fugate DC, Friedrichs CT, Sanford LP. 2007. Lateral dynamics and associated transport of sediment in the upper reaches of a partially mixed estuary, Chesapeake Bay, USA. *Cont. Shelf Res.* 27:679–98

Geyer WR. 1993. The importance of suppression of turbulence by stratification on the estuarine turbidity maximum. *Estuaries* 16:113–25

Geyer WR, MacCready P. 2014. The estuarine circulation. *Annu. Rev. Fluid Mech.* 46:175–97

Geyer WR, Ralston DK. 2015. Estuarine frontogenesis. *J. Phys. Oceanogr.* 45:546–61

Geyer WR, Ralston DK. 2018. A mobile pool of contaminated sediment in the Penobscot Estuary, Maine, USA. *Sci. Total Environ.* 612:694–707

Geyer WR, Signell RP, Kineke GC. 1998. Lateral trapping of sediment in partially mixed estuary. In *Physics of Estuaries and Coastal Seas: Proceedings of the 8th International Biennial Conference on Physics of Estuaries and Coastal Seas*, ed. J Dronkers, MBAM Scheffers, pp. 115–124. Rotterdam, Neth.: Balkema

Geyer WR, Trowbridge JH, Bowen MM. 2000. The dynamics of a partially mixed estuary. *J. Phys. Oceanogr.* 30:2035–48

Geyer WR, Woodruff JD, Traykovski P. 2001. Sediment transport and trapping in the Hudson River estuary. *Estuaries Coasts* 24:670–79

Glangeaud L. 1938. Transport et sédimentation dans l'estuaire et à l'embouchure de la Gironde. Caractères pétrographiques des formations fluviatiles, saumâtres, littorales et néritiques. *Bull. Geol. Soc. Fr.* 8:599–630

Groen P. 1967. On the residual transport of suspended matter by an alternating tidal current. *Neth. J. Sea Res.* 3:564–74

Hansen DV, Rattray M. 1965. Gravitational circulation in straits and estuaries. *J. Mar. Res.* 23:104–22

Hudson AS, Talke SA, Jay DA. 2017. Using satellite observations to characterize the response of estuarine turbidity maxima to external forcing. *Estuaries Coasts* 40:343–58

Huijts KMH, Schuttelaars HM, de Swart HE, Friedrichs CT. 2009. Analytical study of the transverse distribution of along-channel and transverse residual flows in tidal estuaries. *Cont. Shelf Res.* 29:89–100

Huijts KMH, Schuttelaars HM, de Swart HE, Valle-Levinson A. 2006. Lateral entrapment of sediment in tidal estuaries: an idealized model study. *J. Geophys. Res.* 111:C12016

Ianniello JP. 1979. Tidally induced residual currents in estuaries of variable breadth and depth. *J. Phys. Oceanogr.* 9:962–74

Jalón-Rojas I, Schmidt S, Sottolichio A, Bertier C. 2016. Tracking the turbidity maximum zone in the Loire Estuary (France) based on a long-term, high-resolution and high-frequency monitoring network. *Cont. Shelf Res.* 117:1–11

Jay DA, Musiak JD. 1994. Particle trapping in estuarine tidal flows. *J. Geophys. Res.* 99:445–61

Jay DA, Musiak JD. 1996. Internal tidal asymmetry in channel flows: origins and consequences. In *Mixing Processes in Estuaries and Coastal Seas*, ed. C Pattiararchi, pp. 211–49. Washington, DC: Am. Geophys. Union

Jay DA, Orton PM, Chisholm T, Wilson DJ, Fain AM. 2007a. Particle trapping in stratified estuaries: consequences of mass conservation. *Estuaries Coasts* 30:1095–105

Jay DA, Orton PM, Chisholm T, Wilson DJ, Fain AMV. 2007b. Particle trapping in stratified estuaries: application to observations. *Estuaries Coasts* 30:1106–25

Jay DA, Talke SA, Hudson AS, Twardowski M. 2015. Estuarine turbidity maxima revisited: instrumental approaches, remote sensing, modeling studies, and new directions. In *Fluvial-Tidal Sedimentology*, ed. PJ Ashworth, JL Best, DR Parsons, pp. 49–109. Dev. Sedimentol. Vol. 68. Amsterdam: Elsevier

Jay DA, Uncles RJ, Largeir J, Geyer WR, Vallino J, Boynton WR. 1997. A review of recent developments in estuarine scalar flux estimation. *Estuaries* 20:262–80

Kappenberg J, Grabemann I. 2001. Variability of the mixing zones and estuarine turbidity maxima in the Elbe and Weser estuaries. *Estuaries* 24:699–706

Kappenberg J, Schymura G, Fanger HU. 1995. Sediment dynamics and estuarine circulation in the turbidity maximum of the Elbe River. *Neth. J. Aquat. Ecol.* 29:229–37

Kim YH, Voulgaris G. 2008. Lateral circulation and suspended sediment transport in a curved estuarine channel: Winyah Bay, SC, USA. *J. Geophys. Res.* 113:C09006

Klingbeil AD, Sommerfield CK. 2005. Latest holocene evolution and human disturbance of a channel segment in the Hudson River Estuary. *Mar. Geol.* 218:135–53

Knudsen M. 1900. Ein hydrographischer Lehrsatz. *Ann. Hydrogr. Marit. Meteorol.* 28:316–20

Kumar M, Schuttelaars HM, Roos PC. 2017. Three-dimensional semi-idealized model for estuarine turbidity maxima in tidally dominated estuaries. *Ocean Model.* 113:1–21

Lang G, Schubert R, Markowsky M, Fanger HU, Grabemann I, et al. 1989. Data interpretation and numerical modelling of the Mud and Suspended Sediment Experiment 1985. *J. Geophys. Res.* 94:14381–93

Le Hir P, Ficht A, Jacinto RS, Lesueur P, Dupont JP, et al. 2001. Fine sediment transport and accumulations at the mouth of the Seine estuary (France). *Estuaries* 24:950–63

Lerczak JA, Geyer WR. 2004. Modeling the lateral circulation in straight, stratified estuaries. *J. Phys. Oceanogr.* 34:1410–28

Lin J, Kuo AY. 2001. Secondary turbidity maximum in a partially mixed microtidal estuary. *Estuaries Coasts* 24:707–20

MacCready P, Geyer WR. 2010. Advances in estuarine physics. *Annu. Rev. Marine. Sci.* 2:35–58

McAnally W, Mehta A. 2002. Significance of aggregation of fine sediment particles in their deposition. *Estuar. Coast. Shelf Sci.* 54:643–53

McSweeney JM, Chant RJ, Sommerfield CK. 2016. Lateral variability of sediment transport in the Delaware Estuary. *J. Geophys. Res.* 121:725–44

Meade RH. 1969. Landward transport of bottom sediments in estuaries of the Atlantic coastal plain. *J. Sediment. Res.* 39:222–34

Menon MG, Gibbs RJ, Phillips A. 1998. Accumulation of muds and metals in the Hudson River estuary turbidity maximum. *Environ. Geol.* 34:214–22

Mitchell S, Akesson L, Uncles R. 2012. Observations of turbidity in the Thames estuary, United Kingdom. *Water Environ. J.* 26:511–20

Nash DB. 1994. Effective sediment-transporting discharge from magnitude-frequency analysis. *J. Geol.* 102:79–95

Nitsche FO, Kenna TC, Haberman M. 2010. Quantifying 20th century deposition in complex estuarine environment: an example from the Hudson River. *Estuar. Coast. Shelf Sci.* 89:163–74

North EW, Houde ED. 2001. Retention of white perch and striped bass larvae: biological-physical interactions in Chesapeake Bay estuarine turbidity maximum. *Estuaries Coasts* 24:756–69

Panuzio FL. 1965. Lower Hudson River siltation. In *Proceedings of the 2nd Federal Interagency Sedimentation Conference*, pp. 512–50. Jackson, MS: Agric. Res. Serv.

Postma H. 1954. Hydrography of the Dutch Wadden Sea. *Arch. Neerl. Zool.* 10:405–511

Postma H. 1967. Sediment transport and sedimentation in the estuarine environment. In *Estuaries*, ed. GH Lauff, pp. 158–79. Washington DC: Am. Assoc. Adv. Sci.

Postma H, Kalle K. 1955. Die Entstehung von Trübungszonen im Unterlauf der Flüsse, speziell im Hinblick auf die Verhältnisse in der Unterelbe. *Dtsch. Hydrogr. Z.* 8:138–44

Ralston DA, Geyer WR, Lerczak JA. 2008. Subtidal salinity and velocity in the Hudson River estuary: observations and modeling. *J. Phys. Oceanogr.* 38:753–70

Ralston DK, Geyer WR. 2009. Episodic and long-term sediment transport capacity in the Hudson River estuary. *Estuaries Coasts* 32:1130–51

Ralston DK, Geyer WR. 2017. Sediment transport time scales and trapping efficiency in a tidal river. *J. Geophys. Res.* In press. **https://doi.org/10.1002/2017JF004337**

Ralston DK, Geyer WR, Warner JC. 2012. Bathymetric controls on sediment transport in the Hudson River estuary: lateral asymmetry and frontal trapping. *J. Geophys. Res.* 117:C10013

Ralston DK, Warner JC, Geyer WR, Wall GR. 2013. Sediment transport due to extreme events: the Hudson River estuary after tropical storms Irene and Lee. *Geophys. Res. Lett.* 40:5451–55

Richardson JF, Zaki WN. 1954. The sedimentation of a suspension of uniform spheres under conditions of viscous flow. *Chem. Eng. Sci.* 3:65–73

Rouse H. 1939. Experiments on the mechanics of sediment suspension. In *Proceedings of the Fifth International Congress on Applied Mechanics*, pp. 550–54. New York: Wiley & Sons

Sanford LP. 2008. Modeling a dynamically varying mixed sediment bed with erosion, deposition, bioturbation, consolidation, and armoring. *Comput. Geosci.* 34:1263–83

Sanford LP, Suttles SE, Halka JP. 2001. Reconsidering the physics of the Chesapeake Bay estuarine turbidity maximum. *Estuaries Coasts* 24:655–69

Schoellhamer DH. 2000. Influence of salinity, bottom topography, and tides on locations of estuarine turbidity maxima in northern San Francisco Bay. In *Coastal and Estuarine Fine Sediment Transport Processes*, ed. WH McAnally, AJ Mehta, pp. 343–57. Amsterdam: Elsevier

Schoellhamer DH. 2002. Variability of suspended-sediment concentration at tidal to annual time scales in San Francisco Bay, USA. *Cont. Shelf Res.* 22:1857–66

Schoellhamer DH. 2011. Sudden clearing of estuarine waters upon crossing the threshold from transport to supply regulation of sediment transport as an erodible sediment pool is depleted: San Francisco Bay, 1999. *Estuaries Coasts* 34:885–99

Schoellhamer DH, Mumley TE, Leatherbarrow JE. 2007. Suspended sediment and sediment-associated contaminants in San Francisco Bay. *Environ. Res.* 105:119–31

Schuttelaars HM, de Jonge VN, Chernetsky A. 2013. Improving the predictive power when modelling physical effects of human interventions in estuarine systems. *Ocean Coast. Manag.* 79:70–82

Scott K. 1984. *Hindered settling of a suspension of spheres: critical evaluation of equations relating settling rate to mean particle diameter and suspension concentration*. Tech. Rep. 497, Chem. Eng. Res. Group, Counc. Sci. Ind. Res., Pretoria, S. Afr.

Scully ME, Friedrichs CT. 2003. The influence of asymmetries in overlying stratification on near-bed turbulence and sediment suspension in a partially mixed estuary. *Ocean Dyn*. 53:208–19

Scully ME, Friedrichs CT. 2007. Sediment pumping by tidal asymmetry in a partially mixed estuary. *J. Geophys. Res.* 112:C07028

Scully ME, Friedrichs CT, Brubaker JM. 2005. Control of estuarine stratification and mixing by wind-induced straining of the estuarine density field. *Estuaries* 28:321–26

Simenstad CA, Reed D, Jay DA, Prahl F, Small L, Baross JA. 1994. LMER in the Columbia River Estuary: an interdisciplinary approach to investigating couplings between hydrological, geochemical and ecological processes. In *Changing Particle Fluxes in Estuaries: Implications from Science to Management*, ed. KR Dyer, RJ Orth, pp. 437–44. Fredensborg, Den.: Olsen & Olsen

Simpson JH, Brown J, Matthews J, Allen G. 1990. Tidal straining, density currents, and stirring in the control of estuarine stratification. *Estuaries* 13:125–32

Sommerfield CK, Wong KC. 2011. Mechanisms of sediment flux and turbidity maintenance in the Delaware Estuary. *J. Geophys. Res.* 116:C01005

Song D, Wang XH, Cao Z, Guan W. 2013. Suspended sediment transport in the deepwater navigation channel, Yangtze River Estuary, China, in the dry season 2009: 1. Observations over spring and neap tidal cycles. *J. Geophys. Res.* 118:5555–67

Soulsby RL, Wainwright BLSA. 1987. A criterion for the effect of suspended sediment on near-bottom velocity profiles. *J. Hydraul. Res.* 25:341–56

Talke SA, de Swart HE, Schuttelaars HM. 2009. Feedback between residual circulations and sediment distribution in highly turbid estuaries: an analytical model. *Cont. Shelf Res.* 29:119–35

Traykovski P, Geyer WR, Sommerfield CK. 2004. Rapid sediment deposition and fine-scale strata formation in the Hudson estuary. *J. Geophys. Res.* 109:F02004

Trowbridge JH, Butman B, Limeburner R. 1994. Characteristics of the near-bottom suspended sediment field over the continental shelf off northern California based on optical attenuation measurements during STRESS and SMILE. *Cont. Shelf Res.* 14:1257–72

Uncles RJ, Elliott RCA, Weston SA. 1985. Dispersion of salt and suspended sediment in a partly mixed estuary. *Estuaries Coasts* 8:256–69

Uncles RJ, Stephens JA. 1993. The freshwater-saltwater interface and its relationship to the turbidity maximum in the Tamar Estuary, United Kingdom. *Estuaries* 16:126–41

Uncles RJ, Stephens JA, Harris C. 2006. Runoff and tidal influences on the estuarine turbidity maximum of a highly turbid system: the upper Humber and Ouse Estuary, UK. *Mar. Geol.* 235:213–28

Uncles RJ, Stephens JA, Smith RE. 2002. The dependence of estuarine turbidity on tidal intrusion length, tidal range and residence time. *Cont. Shelf Res.* 22:1835–56

Van Leussen W. 1994. *Estuarine macroflocs and their role in fine-grained sediment transport*. PhD Thesis, Univ. Utrecht, Neth.

Van Olphen H. 1977. *An Introduction to Clay Collois Chemistry*. New York: Wiley & Sons

Van Straaten LMJU, Kuenen PH. 1958. Tidal action as a cause of clay accumulation. *J. Sediment. Petrol.* 28:406–13

Vanoni VA. 1946. Transportation of suspended sediment by water. *Trans. Am. Soc. Civil Eng.* 111:67–102

Wang X. 2002. Tide-induced sediment resuspension and the bottom boundary layer in an idealized estuary with a muddy bed. *J. Phys. Oceanogr.* 32:3113–31

Wang X, Byun D, Wang X, Cho Y. 2005. Modelling tidal currents in a sediment stratified idealized estuary. *Cont. Shelf Res.* 25:655–65

Wei X. 2017. *A process-based, idealized study of salt and sediment dynamics in well-mixed estuaries*. PhD Thesis, Delft Univ. Technol., Delft, Neth.

Wellershaus S. 1981. Turbidity maximum and shoaling in the Weser estuary. *Arch. Hydrobiol.* 92:161–98

Winterwerp JC. 1998. A simple model for turbulence induced flocculation of cohesive sediment. *J. Hydraul. Res.* 36:309–26

Winterwerp JC. 2001. Stratification effects by cohesive and noncohesive sediment. *J. Geophys. Res.* 106:22559–74

Winterwerp JC. 2002. On the flocculation and settling velocity of estuarine mud. *Cont. Shelf Res.* 22:1339–60

Winterwerp JC. 2011. Fine sediment transport by tidal asymmetry in the high-concentrated Ems River: indications for a regime shift in response to channel deepening. *Ocean Dyn*. 61:203–15

Winterwerp JC, van Kesteren WGM. 2004. *Introduction to the Physics of Cohesive Sediment Dynamics in the Marine Environment*. Dev. Sedimentol. Vol. 56. Amsterdam: Elsevier

Winterwerp JC, Vroom J, Wang ZB, Krebs M, Hendriks ECM, et al. 2017. SPM response to tide and river flow in the hyper-turbid Ems River. *Ocean Dyn*. 67:559–83

Winterwerp JC, Wang ZB. 2013. Man-induced regime shifts in small estuaries—I: theory. *Ocean Dyn*. 63:1279–92

Winterwerp JC, Wang ZB, van Braeckel A, van Holland G, Kösters F. 2013. Man-induced regime shifts in small estuaries—II: a comparison of rivers. *Ocean Dyn*. 63:1293–306

Winterwerp JC, Wang ZB, Van der Kaaij T, Verelst K, Bijlsma A, et al. 2006. Flow velocity profiles in the lower Scheldt estuary. *Ocean Dyn*. 56:284–94

Wolanski E, Chappell J, Ridd P, Vertessy R. 1988. Fluidization of mud in estuaries. *J. Geophys. Res.* 93:2351–61

Woodruff JD, Geyer WR, Sommerfield CK, Driscoll NW. 2001. Seasonal variation of sediment deposition in the Hudson River estuary. *Mar. Geol.* 179:105–19

Yang Z, de Swart HE, Cheng H, Jiang C, Valle-Levinson A. 2014. Modelling lateral entrapment of suspended sediment in estuaries: the role of spatial lags in settling and M_4 tidal flow. *Cont. Shelf Res.* 85:126–42

Yellen B, Woodruff JD, Ralston DK, MacDonald DG, Jones DS. 2017. Salt wedge dynamics lead to enhanced sediment trapping within side embayments in high-energy estuaries. *J. Geophys. Res.* 122:2226–42

Yoshiyama K, Sharp JH. 2006. Phytoplankton response to nutrient enrichment in an urbanized estuary: apparent inhibition of primary production by overeutrophication. *Limnol. Oceanogr.* 51:424–34

Yu Q, Wang Y, Gao J, Gao S, Flemming B. 2014. Turbidity maximum formation in a well-mixed macrotidal estuary: the role of tidal pumping. *J. Geophys. Res.* 119:7705–24

Zimmerman JTF. 1979. On the Euler-Lagrange transformation and the Stokes drift in the presence of oscillatory and residual currents. *Deep-Sea Res. A* 26:505–20

ANNUAL REVIEWS

Connect With Our Experts

ONLINE NOW!

New From Annual Reviews:

Annual Review of Cancer Biology

cancerbio.annualreviews.org • Volume 1 • March 2017

Co-Editors: **Tyler Jacks**, *Massachusetts Institute of Technology*
Charles L. Sawyers, *Memorial Sloan Kettering Cancer Center*

The *Annual Review of Cancer Biology* reviews a range of subjects representing important and emerging areas in the field of cancer research. The *Annual Review of Cancer Biology* includes three broad themes: Cancer Cell Biology, Tumorigenesis and Cancer Progression, and Translational Cancer Science.

TABLE OF CONTENTS FOR VOLUME 1:

ANNUAL REVIEWS | CONNECT WITH OUR EXPERTS

650.493.4400/800.523.8635 (US/CAN)
www.annualreviews.org | service@annualreviews.org

Annual Review of
Marine Science

Volume 10, 2018

Contents

Errata

An online log of corrections to *Annual Review of Marine Science* articles may be found at http://www.annualreviews.org/errata/marine